European Journal of Advanced Chemistry Research
Vol 5 | Issue 2 | May 2024
ISSN 2684-4478

RESEARCH ARTICLE

Adsorption Behavior Investigation of Congored onto Nano-Magnetic Cupper-Nickel Ferrites Surface

Atyaf Mirdan Kadhem* and Tariq Zbare Jassim

ABSTRACT

Ferrite nanoparticles (NPS) of the structure $CuNiFe_2O_4$ were synthesized, and the auto combustion process was done using sol-gel. Several methods and nanomaterials have been identified using approaches such as Fourier-Transform Infrared Spectroscopy (FT-IR), X-Ray diffraction (XRD), and Filled Emission Scanning Electron Microscopy (FE-SEM). Measurements were made on the impact of temperature, pH, and contraction on the uptake behavior of CR dye. The ideal duration of interaction to achieve balance is 240 min, and the pH levels fall between 3 and 11. When compared to the Freundlich model, the desorption data demonstrated a good connection with the Lengmuir model. The thermodynamic parameters showed that ΔH was an exothermic reaction, ΔG was a spontaneous process, and ΔS had a negative value, indicating that the process was less disorderly and unpredictable.

Submitted: February 07, 2024

Published: May 13, 2024

10.24018/ejchem.2024.5.2.152

Department of Chemistry College of Education for Pure Sciences, University of Basra, Iraq.

***Corresponding Author:**
e-mail: mustafafadil837@gmail.com

Keywords: CR day, Ferrite nanoparticles, Freundlich, Langmuir.

1. Introduction

Conventional methods (coagulation-flocculations biological treatment) do not efficiently remove or degrade dyes found in effluents from many industrial sectors, such as textiles, food, and cosmetics. Many days are not only highly poisonous, but they also hinder light penetration, which prevents receiving water bodies from absorbing oxygen again [1], [2]. Numerous cases have been documented of the carcinogenic effects of dyes on the brain, kidney, liver, and digestive system, as well as on genetic makeup, which can lead to the emergence of cancer in these organs [3]. The carcinogenic effects of working with dye and associated chemicals on industrial workers were reported by Morikawa *et al*. [4].

The traditional techniques for removing dyes include membrane separation [5], coagulation [6], chemical filtration [7], biodegradation [8], demands a lot of energy, produce toxic sludge that needs to be disposed of further, and only removes a portion of the ions [9]. Non-biodegradable coloring, softening, and fixing agents are included in the usually treated industrial effluents released into the environment, which increases the risk of bioaccumulation and bio-magnification [10]. Extensive consideration is being given to the development of innovative and economically sound nanomaterials for various purposes, including natural remediation and contaminant detection. Recent developments suggest that several issues, such as water quality, can be resolved or improved through the use of numerous nanotechnologies, including nanoparticles and nanofiltration, as well as other instruments made possible by this technology's advancement [11], [12].

Recently, it was discovered that spinel ferrites constitute a new family of adsorbents that work well for treating water [13], [14]. Its huge surface area and numerous efficient spots make it appropriate for eliminating pollutants. Because spinel ferrites have excellent super paramagnetic characteristics (SPM), it is easy to extract them from the reaction mixture using an external magnetic field [15], [16]. Studies have been done on spinel ferrites' ability to remove dangerous metals, nutritional salts, and organic substances from water [17]. In general, M Fe_20_4, where M can be any of the following: Fe, Co, Ni, Zu, etc., is the universal for spinel ferrites. Its cubic structure has 32 0-atoms, of which 8 Td (tetrahedral) and 16 oh (octahedral) sites were occupied. When synthesizing nanoparticles of magnetized spinel

ferrites, Their big surface area and small size increase their removal capacity [18]. Cobalt and zinc ferrite magnetic highly crystalline and evenly sized nanoparticles were prepared by a variety of synthetic procedures, including the coprecipitation method and precipitation method [19], [20]. the sol-gel auto-combustion approach [21], the hydrothermal method [22], and the sol-gel method [23].

In the current work, local citric acid was used in the sol-gel auto-combustion approach to synthesize $CuNiFe_20_4$ ferrite sample. Compared to the traditional synthesis of technologies, this technique, as a fuel factor and surfactant, is thought to be more economical and environmentally beneficial.

2. Methods

2.1. Synthesis of $CuNiFe_2O_4$ Nanoparticles

The following outlines the way the $CuNiFe_2O_4$ synthesis process was carried out:

In twenty-five milliliters of citric acid solution, 14.54 g of $Fe(NO_3)_3.9H_2O$ (M.W 404 g/mol), 2.6173 g of $Ni(NO_3)_2.6H_2O$ (M.W 290.69 g/mol), and 2.1747 g of $Cu(NO_3)_2.3H_2O$ (M.W 241 g/mol) were mixed and dissolved. To maintain the pH of the mixture was maintained at 7.0 while constantly stirring it with a magnetic stirrer, ammonia solution (NH_4OH) was added. After 30 min of constant stirring at 80 °C, the clear solution fully gelled. To achieve a consistent weight, desiccate in an oven at 80 °C. Grind to a fine powder and then calcined for 3 h at 600 °C in an air-filled furnace.

2.2. Characterization

Numerous novel, extremely effective cutting-edge, widely-has used that are incredibly effective. FESEM-EDX, or energy dispersive X-ray spectroscopy, provides these instances. Fourier transform infrared (FT-IR), and x-ray diffraction (XRD).

2.3. Adsorption Studies

A stock solution of congo red dye was prepared by dissolving 0.1 g of dye in 100 ml of deionized water. Several diluted solutions were then made from this concentration to find the perfect pH buffer solution, which was utilized to maintain the pH at (3–11). The ideal contact time (5–600 min) was found using the batch method. 50 ml of the dye solution containing 50 mg/L was mixed with 0.2 g of the absorbent, which was then placed in 100 ml flasks. Using an orbital shaker for equilibration, different temperatures (10 °C, 20 °C, 30 °C, and 50 °C) were used. 120 rpm was the rate of agitation; after centrifuging the mixture, a UV-vis spectrophotometer (vv-1200 spectrophotometer) was used to measure the dye's concentration. Equations were utilized to compute the equilibrium uptake of CR dye and the elimination efficiency:

$$\%\, Removal = \frac{(Co - Ce)}{Co} \times 100 \tag{1}$$

$$Qe = \frac{(Co - Ce)}{m} \tag{2}$$

2.4. Thermodynamic Parameters

After different concentrations ranging from 5 to 50 mg/l were produced from the stock solution of CR dye and placed in flasks, 0.2 g of $CuNiFe_2O_4$ was added to each concentration. The flasks were shattered at 120 rpm within the proper balancing time at 10 °C, 20 °C, 30 °C, and 50 °C of temperature. After centrifuging the mixture, the concentration of CR dye was ascertained. Eqs. (3)–(5) were utilized to compute the fluctuations in free energy, ΔG, enthalpy ΔH, and entropy ΔS associated with the adsorption process by the values of the slope and the intersection [24].

$$\Delta G = -RTlnK \tag{3}$$

$$K = \frac{C\,solid}{C\,liquid} \tag{4}$$

$$lnk = \frac{\Delta S}{R} - \frac{\Delta H}{RT} \tag{5}$$

3. Results and Discussion

3.1. FT-IR Spectroscopy

Fig. 1 shows the FTIR spectra of the material that has been determined at 600 °C. Many absorption peaks may have been recorded in the range of 400–4000 cm^{-1} in the infrared spectrum. The stretching vibration of the hydroxide (OH) bond, which represents the adsorption of water on ferrite, may be the reason of the peak seen at 3415 cm^{-1} [25]. Spinel Ferrite is identified in the 400–600 cm^{-1} range by (Cu–0), (Ni–0), and (Fe–0) is stretching vibration [26].

The structural analysis of the sample heated at 600 °C was done by XRD Fig. 2. The phase analysis of size controlled $CuNiFe_2O_4$ is compared with (JCPDS NO 34-0425), which shows that the major diffraction peaks at 20 values corresponding to 111, 220, 311, 222, 400, 420, 511, and 440 of pure structure miller planes are in good agreement with the standard Fe_2O_4. The XRD analysis results from the current study is in good agreement with the findings that have been published. Using the Debye-Scherrer equation, the crystal sizes for the X-ray spectra were determined:

$$\tau hkl = \frac{(K \times \lambda)}{(\beta\, hkl) \times cos(\theta hkl)} \tag{6}$$

where τ is the particle size perpendicular to the natural line of (hkl) plane, β hkl is the full width at half maximum, βhkl is the Bragg angle of (hkl) peak, K is constant equal to 0.9 and λ is wavelength of the X-ray [27]. The particle size of nanoparticles calculated is about 33.84 nm $CuNiFe_2O_4$.

3.2. Surface Morphology and Elemental Analysis

The use of (FESEM) is essential for the study of surface morphology. The $CuNiFe_2O_4$ particles appeared in the FESEM micrographs to be irregularly formed agglomerates that were tightly packed to gather. During the scanning process in this method, by interacting with the sample surface, the electron beam produces a distinct pattern that can be used for identifying surface attributes. One or more of the following steps may take place during the creation of $CuNiFe_2O_4$ particles: as a result of (a) the synthesis of $CuNiFe_2O_4$ via growth and nucleation of surface-free energy is reduced; (b) the element crystals aggregating due to the molecular attraction of distinct scale forces. Surface-free energy is reduced as a result. Aggregation results from the continual residual supersaturation that drives the

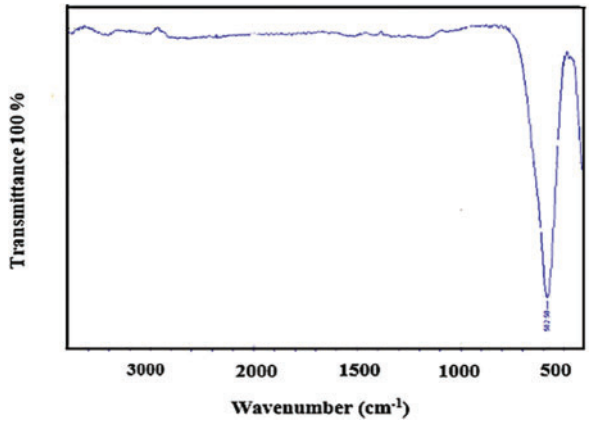

Fig. 1. FT-IR spectra of $CuNiFe_2O_4$.

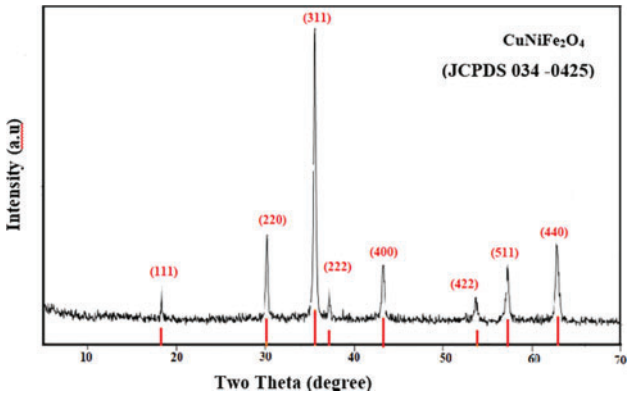

Fig. 2. XRD spectrum of $CuNiFe_2O_4$.

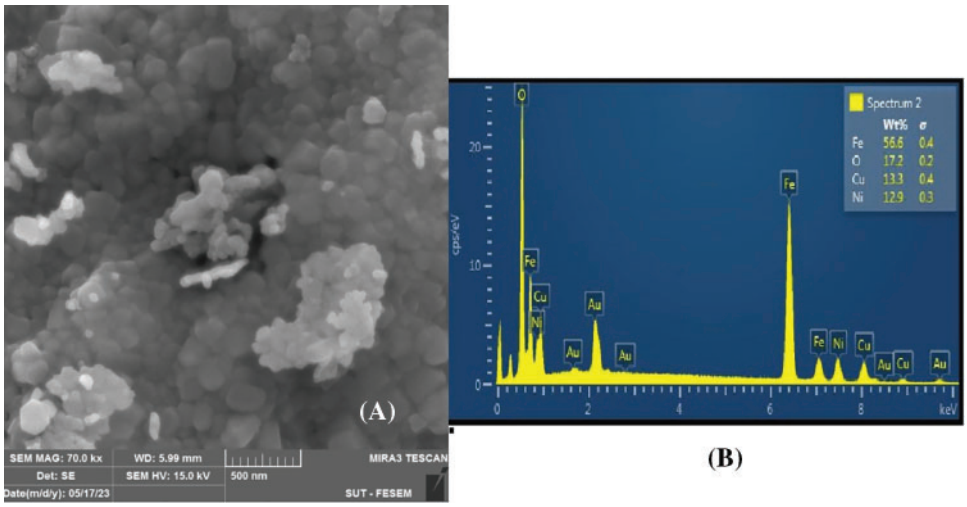

Fig. 3. $CuNiFe_2O_4$: (A) FESEM micrographs of $CuNiFe_2O_4$ and (B) EDX of $CuNiFe_2O_4$ annealed at 600 °C.

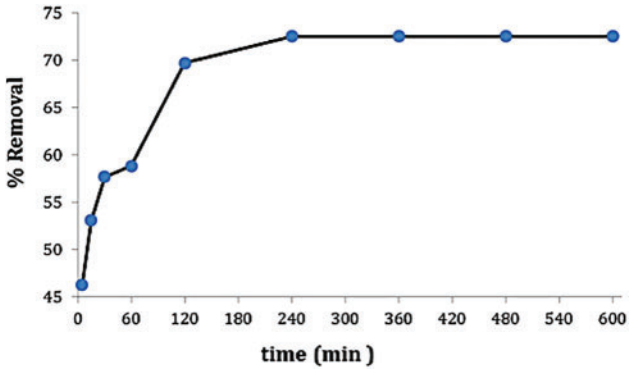

Fig. 4. Influence of CR dye contact time on $CuNiFe_2O_4$.

formation of new crystals inside the aggregates. Subsequently, the agglomerated particles combine with more particles to form secondary particles, which grow in size. This agglomerated particle aggregates to generate secondary particles, which is how the particle size increases. The presence of Cu and Ni in the samples was confirmed by EDX data, indicating that the procedure used to manufacture $CuNiFe_2O_4$ was appropriate. $CuNiFe_2O_4$ with a pure crystal structure was confirmed by XRD, FTIR, and EDX investigation. Fig. 3 shows the EDX photos for Cu, Ni, Fe, and O.

3.3. Adsorption Studies

At a constant temperature of 25 °C, the impact of contact time on the CR dye adsorption was investigated throughout a range of periods (5–600 min). Fig. 4 illustrates how extending the contact time until equilibrium results in an increase in the elimination percentage of CR dye. The large adsorption surface area that is appropriate for the attachment of the CR dye is the reason why the initial adsorption amount was essential. Lastly, equilibrium is stabilized, and the adsorption rate is slower, most likely as a result of active site saturation [28], [29]. The equilibrium time was found to be a duration of 240 min, and 72.5% of the dye was removed.

3.4. Effect of pH on the Adsorption

pH is one of the main factors affecting the dye's adsorption onto the adsorbent. The impact of pH on CR dye adsorption onto $CuNiFe_2O_4$ nanoparticles at different pH (3-11) was investigated using an initial concentration of 50 mg/l, a contact time of 240 min, and an amount of nanoparticle adsorbent of 0.2 g at 25 °C (Fig. 8). The findings demonstrated that when pH accelerates between 3 and 11 (see Fig. 5), the removal percentage of CR decreases from 85% to 20%. At acidic mediums (low pH), the active sites acquire a positive charge, so at pH3, the positively charged surface of $CuNiFe_2O_4$ and the negatively charged anionic CR dye exhibit a notably strong electrostatic interaction. The number of positively charged sites reduced as the system's pH increased, which in turn caused the adsorption capacity in the base medium to decrease [30].

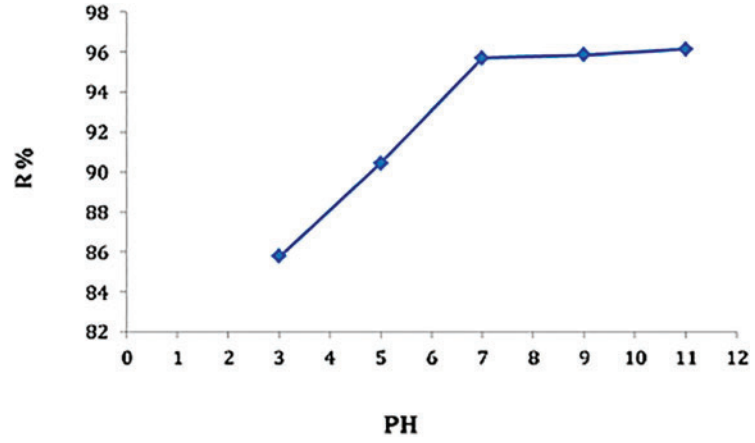

Fig. 5. Influence of pH on CR dye adsorption on $CuNiFe_2O_4$.

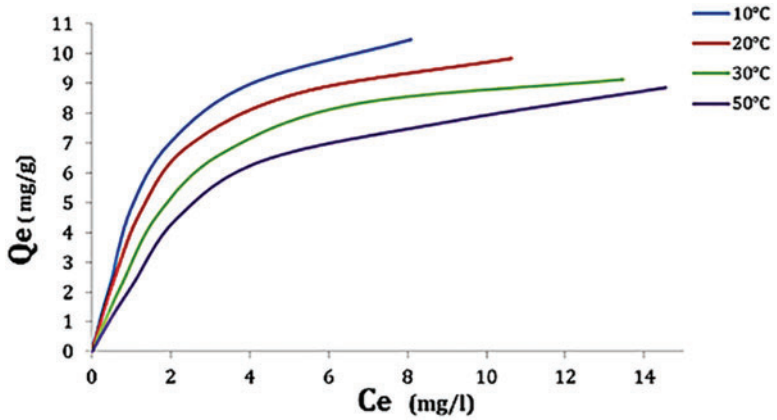

Fig. 6. Shows the dye adsorption isotherm on $CuNiFe_2O_4$ at different temps.

3.5. Adsorption Isotherm

An array of temperatures, 10 °C, 20 °C, 30 °C, and 50 °C, was chosen to evaluate the ability of $CuNiFe_2O_4$ nanoparticles to extract CR dye from their aqueous solution. Fig. 6 shows the general shape of the dye adsorption isotherms, with the amounts adsorbed displayed as a function of equilibrium concentration (Ce) at 10 °C, 20 °C, 30 °C, and 50 °C on nanoparticles $CuNiFe_2O_4$ (Qe).

The form of the CR dye adsorption isotherm on $CuNiFe_2O_4$ is in accordance with the Giles categorization (s-type). As the molten layer is actually adsorbed, where additional quantities are set, the s-curve shows that the flat or vertical orientation of the molecules in the adsorbent layer have a significant attraction to one another [31]. The Freundlich and Langmuir isotherm was used in practice to apply the adsorption results. To track the effect, Freundlich's Eq. (7) and Langmuir's Eq. (8) were applied [32], and Table I displays the isotherm adsorption data:

$$Log\ Qe = log\ Kf + \frac{1}{n} log\ Ce \tag{7}$$

$$T\frac{Ce}{Qe} = \frac{1}{Qmb} + \frac{Ce}{Qm} \tag{8}$$

Where Kf is a function of adsorption capacity an n is the adsorption intensity. Qm is the maximum adsorption capacities (mg/g) and B is related to the sorption energy. The Freundlich and Langmuir isotherm are applied on the experimental data of the adsorption of CR dye on $CuNiFe_2O_4$ by plotting (Ce/Qe) versus (Ce) and (log Qe) versus (log Ce), respectively (Figs. 7 and 8).

According to Table I results, the Langmuir model's R^2 values for the adsorption process onto $CuNiFe_2O_4$ are closer to unity than the Freundlich model's. This indicates that the Langmuir model was more effective than the Freundlich model in characterizing the CR dye adsorption on $CuNiFe_2O_4$ nanoparticles. The findings further demonstrate that the linear (Ce/Qe) against (Ce) relationship in Fig. 7 indicates that the Langmuir isotherms are more suitable for this system than the Freundlich [33].

TABLE I: Shows the Effects when Applying the Freundlich and Langmuir Isotherms on the System for Study

	Temperature (°C)	Langmuir			Freundlich		
		Qm	B	R^2	Kf	n	R^2
CR dye	10	13.247	0.499	0.9935	3.733	1.630	0.9352
	20	11.837	0.495	0.9971	3.292	1.747	0.9310
	30	11.155	0.375	0.9929	2.649	1.717	0.9223
	50	11.210	0.262	0.9928	2.173	1.667	0.9373

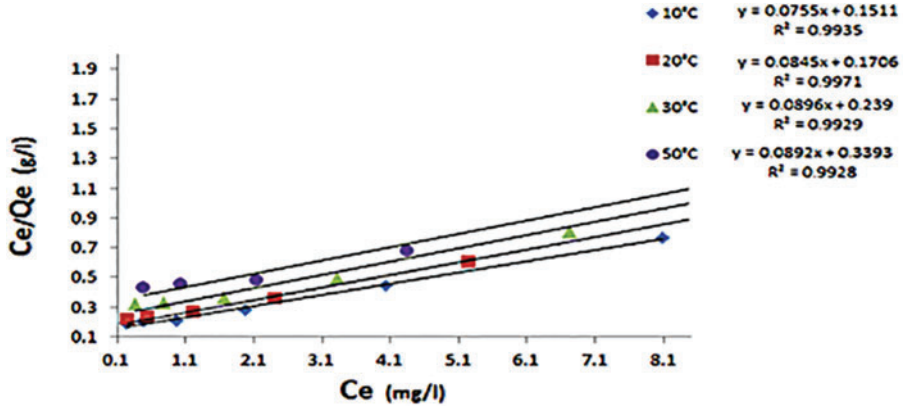

Fig. 7. At various temperatures, the linear form of the Langmuir isotherm of CR dye on $CuNiFe_2O_4$.

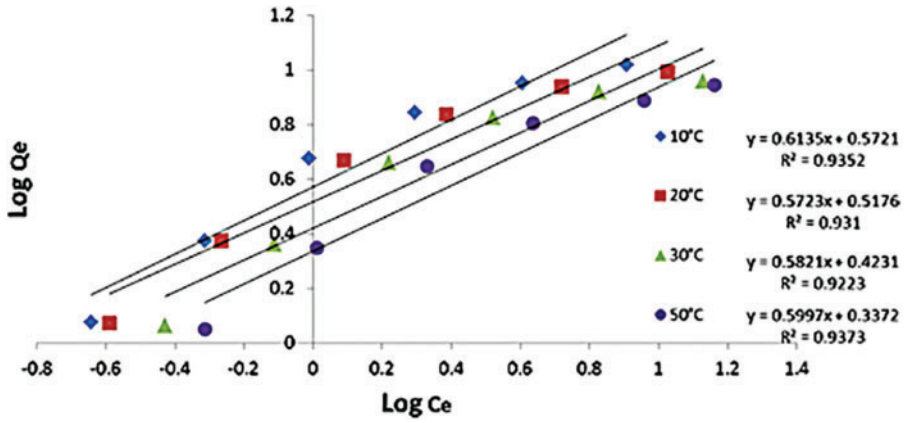

Fig. 8. Freundlich isothermal CR dye CuNi Fes Oy at various temperatures in linear form.

3.6. Thermodynamic Study

Using a range of starting concentrations, the impact of temperature on the adsorption of CR dye onto $CuNiFe_2O_4$ was studied in the range of 10 °C–50 °C. The enthalpy change (ΔH), entropy change (ΔS), and Gibbs energy change (ΔG) thermodynamic parameters can be applied to approximate the adsorption process' efficiency using Eqs. (3)–(5):

Can be calculated based on the resulting slope and intercept of Eq. (4). Table II lists the thermodynamic parameters for the temperature ranges under investigation.

TABLE II: Thermodynamic Function for Adsorption of Studied Dye

	Co (mg/l)	Equilibrium constant (K)				$-\Delta G$ (KJ.mol^{-1})				ΔH (KJ.mol^{-1})	ΔS (KJ.mol^{-1}K^{-1})
		Temperature (°C)				Temperature (°C)					
		10	20	30	50	10	20	30	50		
CR dye	5	20.929	18.455	12.477	9.309	7.378	7.068	6.758	6.138	−16.151	−0.031
	10	19.618	17.450	11.970	8.727	7.357	7.042	6.732	6.112	−16.125	−0.031
	20	19.597	15.286	11.070	8.337	7.039	6.709	6.379	5.719	−16.378	−0.033
	30	14.220	11.355	8.052	5.909	6.491	6.121	5.751	5.011	−16.962	−0.037
	40	8.930	6.608	4.957	3.402	5.201	4.741	4.281	3.361	−18.219	−0.046
	50	5.184	3.704	2.715	2.438	3.909	3.549	3.189	2.469	−14.097	−0.036

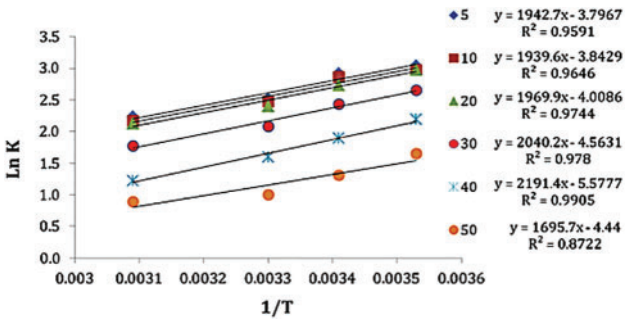

Fig. 9. Plot of lnk against 1/T for $CuNiFe_2O_4$ adsorption of CR dye.

It was discovered that the lnk against 1/T plots were linear, and the adsorption on $CuNiFe_2O_4$ nanoparticles had a correlation coefficient (R^2 = 6.8722–0.9905) (Fig. 9). Table II demonstrates that ΔG was negative across the board, suggesting that the adsorption process occurs spontaneously [34]. The adsorption process is exothermic, as indicated by the negative value of ΔH, and the solid-solution interface is thought to be less disorderly and unpredictable when ΔS is negative [35].

4. Conclusion

$CuNiFe_2O_4$ nanoparticle ferrites were generated in the current work using a sol-gel auto-combustion approach, and the sample was baked at 600 °C to produce a single-stage spinel ferrite. The effects of temperature, pH, and contact time, among other factors, on the ability of adsorption were investigated. For CR dye, its contact duration was 240 min. The maximum percentage reduction of 85% was attained at pH = 3. The pseudo-second order kinetics rate expression for the adsorption kinetics was found to fit the equilibrium data, which in turn followed the Langmuir isotherm model. Thermodynamic investigation shows the adsorption system's exothermic and spontaneous character. The produced chemical is thought to be of great importance for protecting the environment since it can be used as a dye adsorbent.

Conflict of Interest

The authors declare that they do not have any conflict of interest.

References

[1] Ramos MDN, Cláudio CC, Rezende PHV, Santos LA, Cabral LP, Mesquita PL, *et al*. Click on the screen to display the content of the industry's influence on your text in Brazil. *Revista Virtual de Quimica*. 2020a;12:913–29.
[2] Tkaczyk A, Mitrowska K, Posyniak A. Synthetic organic dyes as contaminants of the aquatic environment and their implications for ecosystems: a review. *Sci Total Environ*. 2020;717:137222.
[3] Li E, Li A, He XXL-2, Wang Y, Sia I. Synthesis of AgRtMofs nand composite and it photocatalytic activity. *Polyhedr*. 2019;165:31–7.
[4] Morikawa Y, Shiomi K, Ishihara Y, Matsuura N. Triple primary cancers Involving kidney, urinary bladder, and liver in a dye worker. *Am J Ind Med*. 1997;31:44.
[5] Jin J, Du X, Yu J, Qin S, He M, Zhang K, *et al*. High performance Manofiltration membrane based on SMA-PEI cross-linked coating for dye/salt separation. *J Membr Sci*. 2020;611:118307.
[6] Suhan MBK, Shuchi SB, Anis A, Haque Z, Islam MS. Comparative X degradation study of remazol black B dye using electro-coagulation and electro-Fenton process: kinetics and cost analysis. *Environ Nanotechnol*. 2020;14:100335.
[7] Kim SE, Tieu MV, Hwang SY, Lee MH. Magnetic particles: their applications from sample preparations to biosensing platforms. *Micromachines*. 2020;11(3):302. doi: 10.3390/mi11030302.
[8] Sonwani RK, Swain G, Giri BS, Singh RS, Rai BN. Biodegradation of Congo red dye in a moving bed biofilm reactor: performance evaluation and kinetic modelling. *Bioresour Technol*. 2020;302:122811.
[9] Wang T, Xue Y, Zhou M, Liang A, Liu J, Mei M, *et al*. Effect of addition of rice husk on the fate and speciation of heavy metals in the bottom ash during dyeing sludge incineration. *J Clean Prod*. 2020;244:118851. doi: 10.1016/j.jclepro.2019.118851.
[10] Nandhini NT, Rajeshkumar S, Mythili S. The possible mechanism of eco-friendly synthesized NPs on hazardous dyes degradation. *Biocatal Agric Bio-Technol*. 2019;19:101138.
[11] Jurgen S, Joydeep D. Nanotechnology in environmental protection and pollution. *J Sci Technol Adv Mat*. 2005;6(1): 219–20.
[12] Salman GK, Bohan AJ, Jaed GM. Use of nano-magnetic material for removal of heavy metals from wastewater. *J Eng Technol*. 2017;35(9):903–8.
[13] Kefeni KK, Mamba BB, Msagati TA. Application of spinel ferrite nanoparticles in water and wastewater treatment. A review. *J Sep Purif Technol*. 2017;188(1):399–422.
[14] Chinh VT, Dang VQ, Hoai PN, Tuan NT, Duong D. Effective removal of Pb(II) from aqueous media by a new design of Cu-Mg binary ferrite. *J Am Chem Soc*. 2020;5(2):7298–306.
[15] Baig RB, Varma RS. Magnetically retrievable catalysts for organic synthesis. *Chem Commun*. 2013;49(1):752–70.

[16] Nasir RB, Nadagouda MN, Varma RS. Magnetically retrievable catalysts for asymmetric synthesis. *J Coord Chem Rev*. 2015;287(1):137–56.
[17] Roonasi P, Nezhad AY. Comparative study of a series of ferrite nanoparticles as heterogeneous catalysts for phenol removal at neutral pH. *J Mat Chem Phys*. 2016;172(2):143–9.
[18] Cafer TY, Mayo JT, William WY, Arjun P, Joshua CF, Sujin Y, *et al*. Low-field magnetic separation of monodisperse Fe_3O_4 nanocrystals. *Sci*. 2006;314(1):964–7.
[19] Mahboubeh H, Fatemeh Z, Zahra JR, Zohreh A. Synthesis of cobalt ferrite ($CoFe_2O_4$) nanoparticles using combustion, coprecipitation, and precipitation methods: a comparison study of size, structural, and magnetic properties. *J Magn Magn Mater*. 2014;371(1):43–8.
[20] Baykal A, Deligoz H, Sozeri H, Durmus Z, Toprak MS. Triethylene glycol stabilized $CoFe_20_4$ nanoparticles. *J Supercond Nov Magn*. 2012;25(1):1879–92.
[21] Ismat B, Nosheen N, Munawar I, Shagufta K, Haq N, Shazia N, *et al*. Green and eco-friendly synthesis of cobalt-oxide nanoparticle: characterization and photo-catalytic activity. *J Adv Powder Technol*. 2017;28:2035–43.
[22] Zhao D, Wu X, Guan H, Han E. Study on supercritical hydrothermal synthesis of $CoFe_20_4$ nanoparticles. *J Supercrit Fluids*. 2007;42(1):226–33.
[23] Sivakumar M, Kanagesan S, Babu RS, Jesurani S, Velmurugan R. Synthesis of $CoFe_20_4$ powder via PVA assisted sol-gel process. *J Mat Sci: Mat Electron*. 2012;23(5):1045–9.
[24] Ge H, Ma Z. Microwave preparation of triethylenetetramine modifed graphene oxide/chitosan composite for adsorption of Cr (VI). *J Carbo, Poly*. 2015;131:280–7.
[25] Anandan K, Rajendran V. Morphological and size effects of NiO nanoparticles via solvothermal process and their optical properties. *Mat Sci Semicond Process*. 2011;14(1):43–7.
[26] Kareem SHJ, Rajeh AAH. The effect of catalyst type on the microstructure and magnetic properties of synthesized hard cobalt ferrite. *Nanoparticles*. 2018;26(4):282–91.
[27] Cullity BD. *Elements of X-Ray Diffraction*. 2nd ed. London: Addison-Wesley; 1978.
[28] El-Ashtoukhy E, Amina NK, Abdelwahab O. Removal of lead (II) and copper (II) from aqueous solution using pomegranate peel as a new adsorbent. *J Desalin*. 2008;223(1):162–73.
[29] Pehlivan E, Altun T, Parlayıcı S. Utilization of barley straws as biosorbents for Cut and Pb ions. *J Hazard Mater*. 2009;164(2):982–6.
[30] Pan S, Yu Q, Yu L, Xu Y, Liu R. Preparation and anti-microbial performance of Ni 0.5 Zn 0.5 Fe_2O_4@ Ag nanocomposites. *J Inorg Organomet Polym Mater*. 2021;31:875–85.
[31] Giles CH, MamEwans TH, Nakhwa SN, Smith D. Studies in adsorption. A system of classification of solution adsorption isotherms, and its use in diagnosis of adsorption mechanisms and in measurement of specific surface areas of solids. *J Chem Soc*. 1960;786:3973–93.
[32] Veena M, Robert HH. The Role of F-400 granular activated carbon in scavenging dissolved copper ions from aqueous solution. *J Energeia*. 2002;13:1–4.
[33] Haider IM. *The Study of Adsorption Efficiency of Tea and Coffee Powder For Removal of Some Heavy Metals From Aqueous Solution Lybian Academy*. Misurata University; 2019, pp. 73–1.
[34] Hefne JA, Mekhemer WK, Alandis NM, Aldayel OA, Alaivan T. Kinetic and thermodynamic study of the adsorption of Pb(II) from aqueous solution to the natural and treated bentonite. *International Journal of Physical Sciences*. 2008;3(11):281–288.
[35] Gregg S-J, Wsink K-S. *Adsorption Surface Area and Porosity*. 2nd ed., London: Academic press; 1982, pp. 61–84.